Supra-Monolayer Coverages on Small Metal Clusters and Their Effects on H_2 Chemisorption Particle Size Estimates

Abdulrahman S. Almithn and David D. Hibbitts*

Department of Chemical Engineering, University of Florida, Gainesville, Florida, 32611, United States

*Corresponding author: hibbitts@ufl.edu

Supporting Information

Table of Contents

List of Figures

S1. Density functional theory models

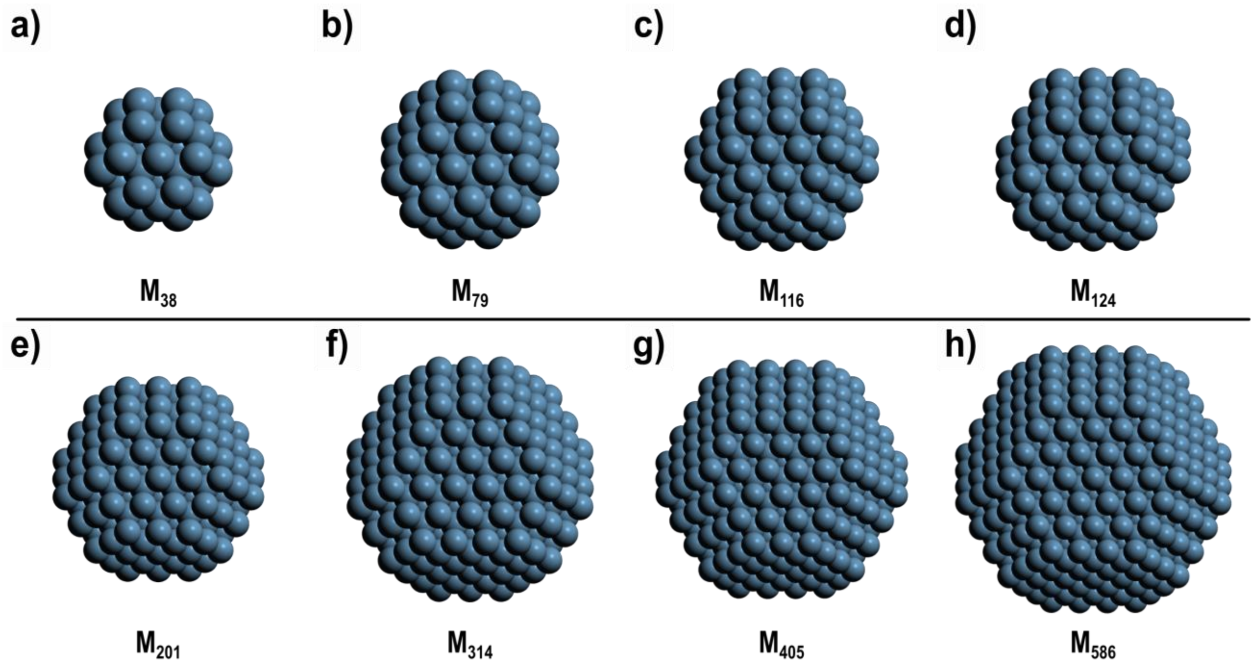

Figure S1. Structural models of all cubo-octahedral particles examined in this study.

S2. H filling pathways for Ir particles*

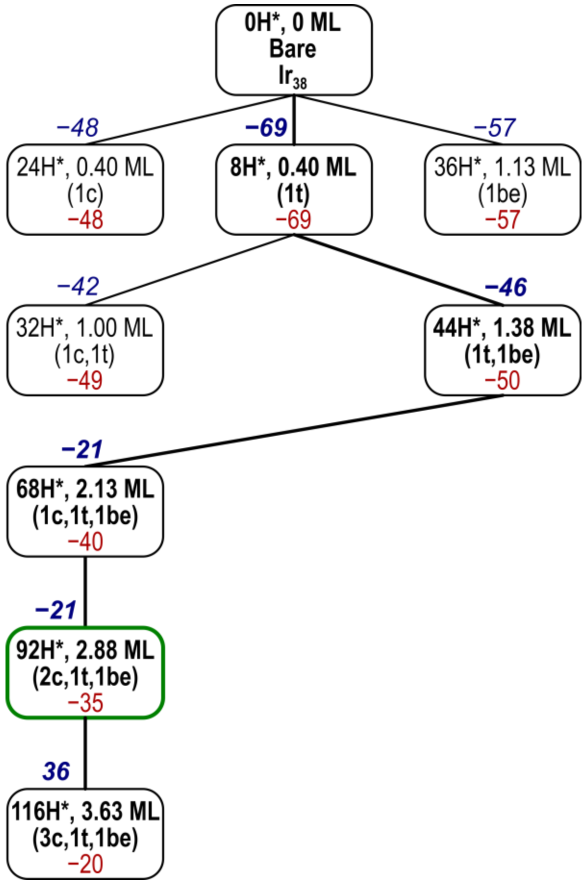

Scheme S1. The minimum energy pathway to fill the Ir_{38} particle (bold). Average H* binding energies ($\Delta\overline{E}$, red) and average differential binding energies ($\Delta\overline{E}_{\mathrm{diff}}$, blue) are shown in kJ mol^{-1}. Each state shows the number of H* atoms, the H* coverage, and the occupancy of corner (c), edge (e), terrace (t), and bridging-edge (be) H* sites.

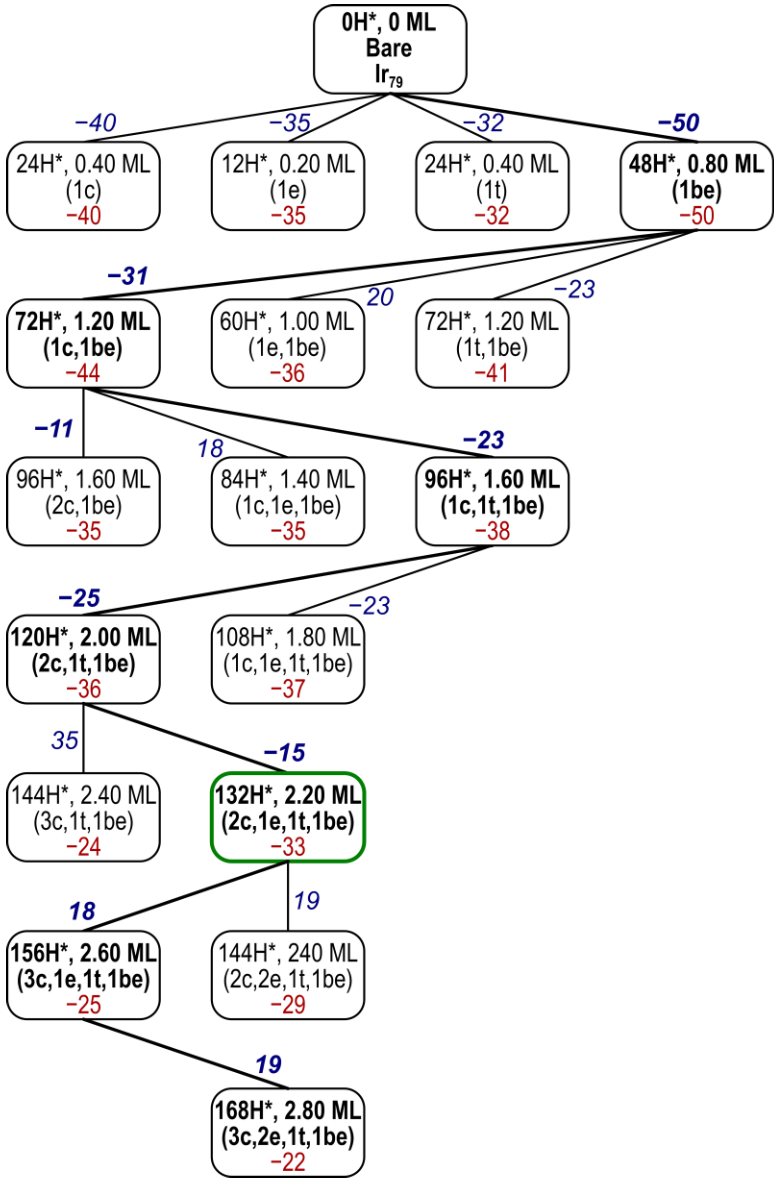

Scheme S2. The minimum energy pathway to fill the Ir_{79} particle (bold). Average H* binding energies ($\Delta\overline{E}$, red) and average differential binding energies ($\Delta\overline{E}_{\mathrm{diff}}$, blue) are shown in kJ mol^{-1}. Each state shows the number of H* atoms, the H* coverage, and the occupancy of corner (c), edge (e), terrace (t), and bridging-edge (be) H* sites.

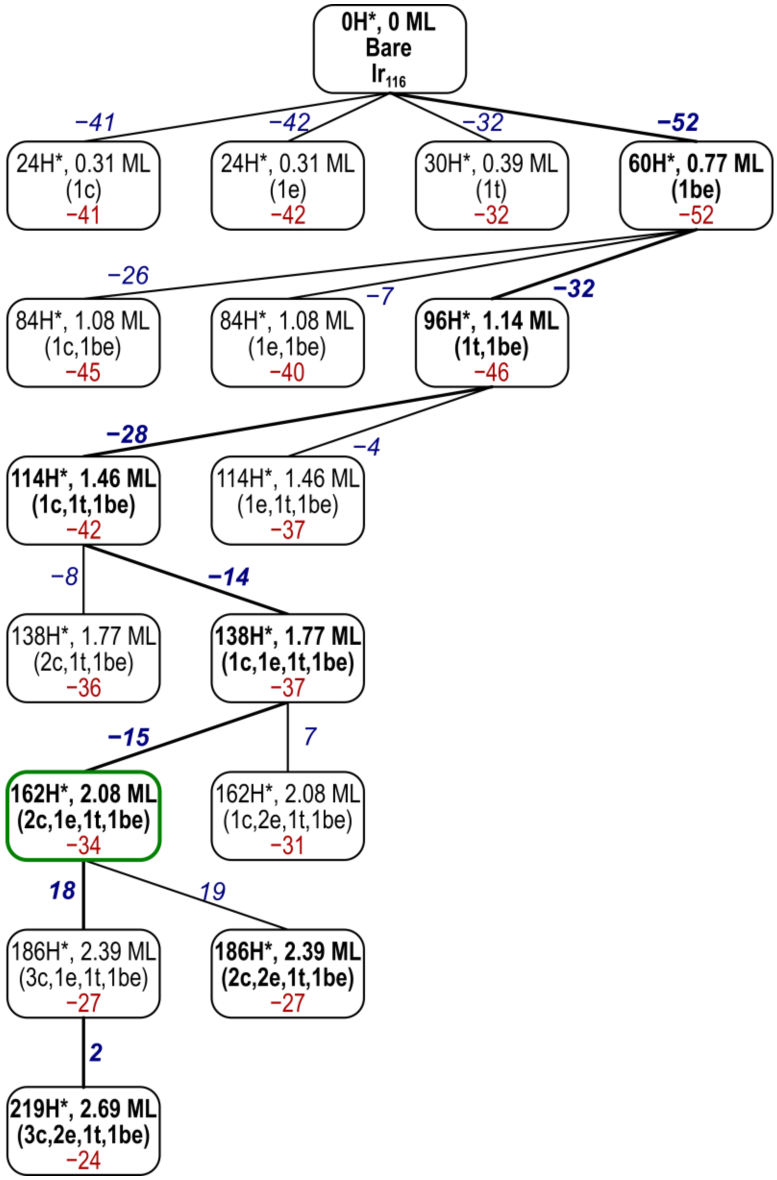

Scheme S3. The minimum energy pathway to fill the Ir_{116} particle (bold). Average H* binding energies ($\Delta\overline{E}$, red) and average differential binding energies ($\Delta\overline{E}_{\mathrm{diff}}$, blue) are shown in kJ mol^{-1}. Each state shows the number of H* atoms, the H* coverage, and the occupancy of corner (c), edge (e), terrace (t), and bridging-edge (be) H* sites.

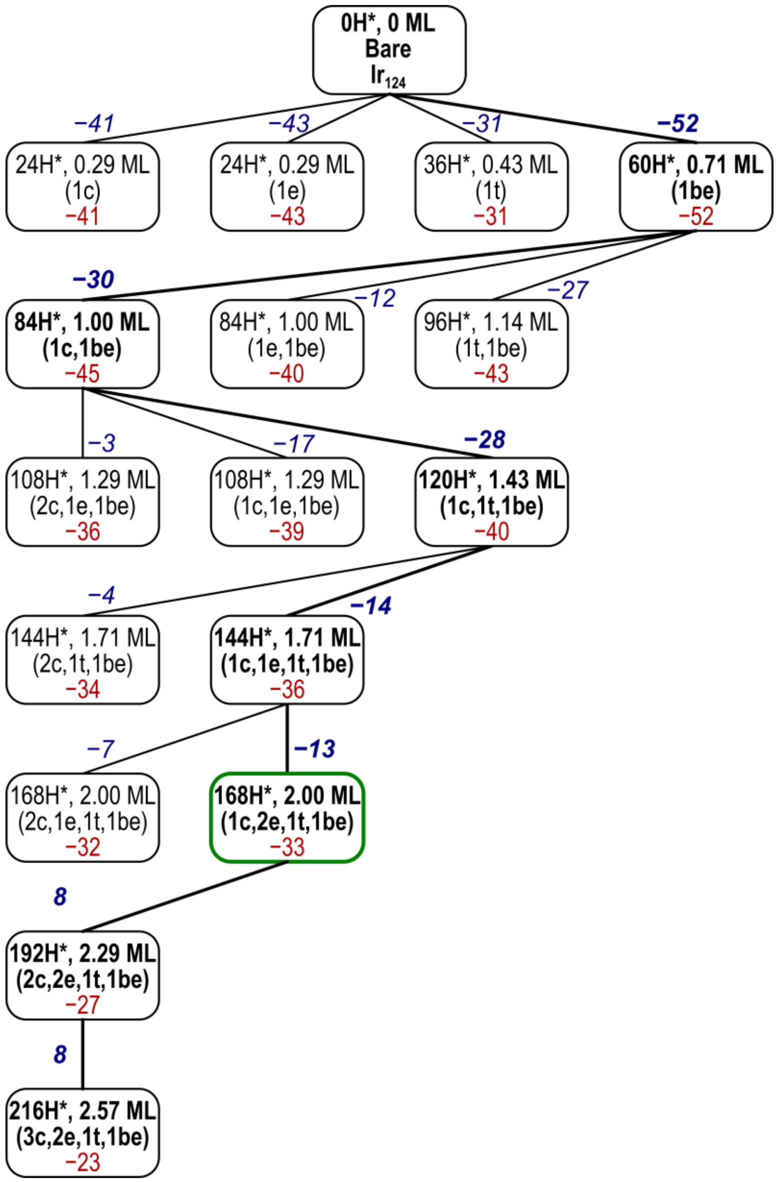

Scheme S4. The minimum energy pathway to fill the Ir_{124} particle (bold). Average H* binding energies ($\Delta\overline{E}$, red) and average differential binding energies ($\Delta\overline{E}_{diff}$, blue) are shown in kJ mol^{-1}. Each state shows the number of H* atoms, the H* coverage, and the occupancy of corner (c), edge (e), terrace (t), and bridging-edge (be) H* sites.

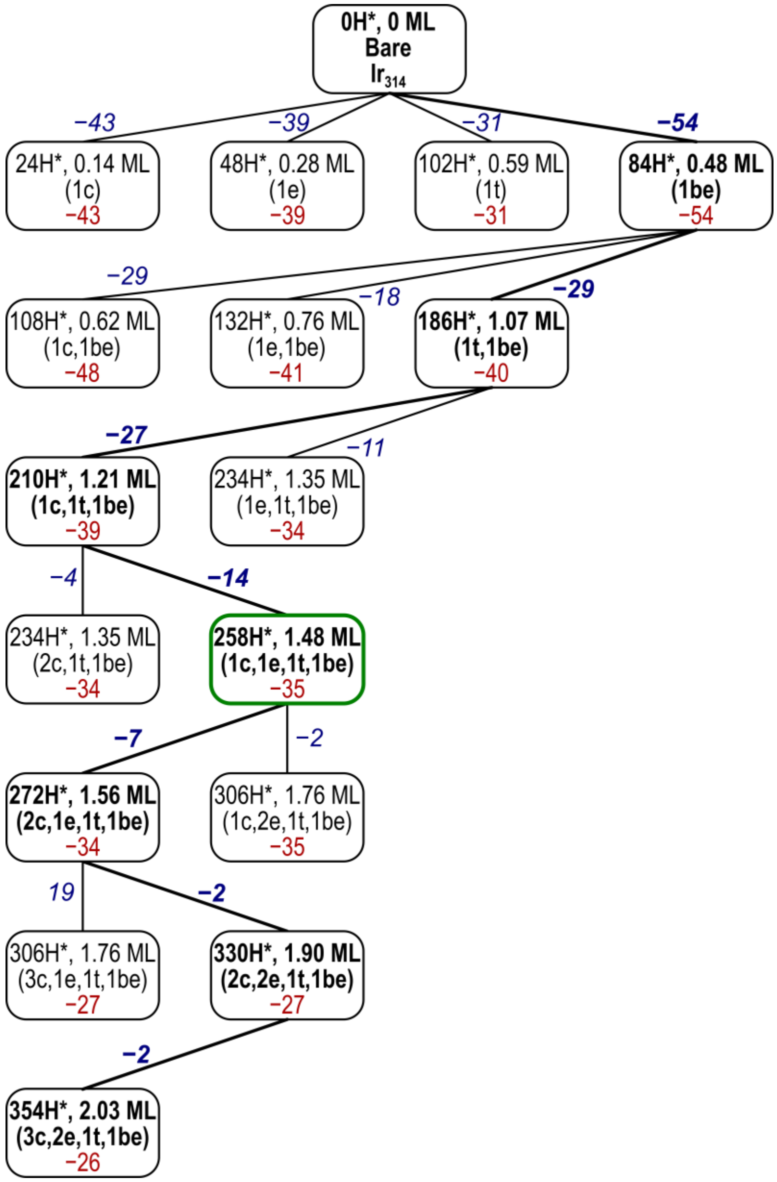

Scheme S5. The minimum energy pathway to fill the Ir_{314} particle (bold). Average H* binding energies ($\Delta\overline{E}$, red) and average differential binding energies ($\Delta\overline{E}_{\text{diff}}$, blue) are shown in kJ mol^{-1}. Each state shows the number of H* atoms, the H* coverage, and the occupancy of corner (c), edge (e), terrace (t), and bridging-edge (be) H* sites.

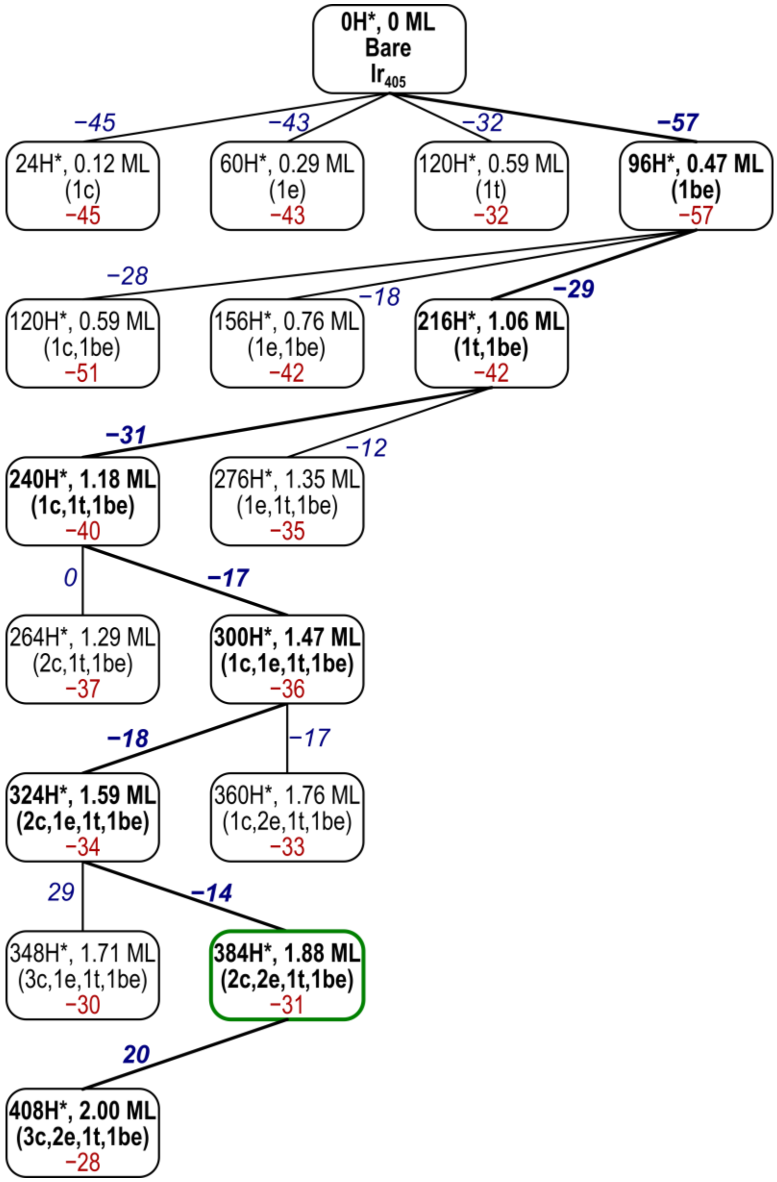

Scheme S6. The minimum energy pathway to fill the Ir_{405} particle (bold). Average H* binding energies ($\Delta\overline{E}$, red) and average differential binding energies ($\Delta\overline{E}_{\text{diff}}$, blue) are shown in kJ mol^{-1}. Each state shows the number of H* atoms, the H* coverage, and the occupancy of corner (c), edge (e), terrace (t), and bridging-edge (be) H* sites.

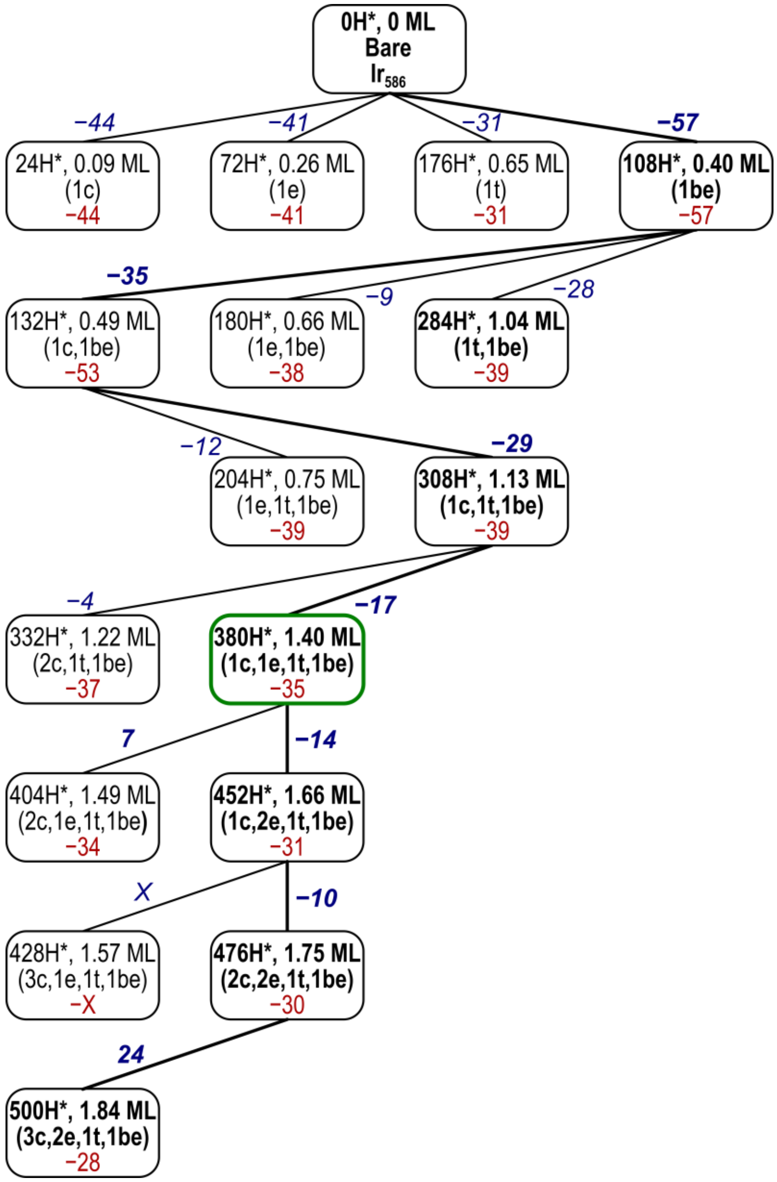

Scheme S7. The minimum energy pathway to fill the Ir_{586} particle (bold). Average H* binding energies ($\Delta\overline{E}$, red) and average differential binding energies ($\Delta\overline{E}_{\mathrm{diff}}$, blue) are shown in kJ mol^{-1}. Each state shows the number of H* atoms, the H* coverage, and the occupancy of corner (c), edge (e), terrace (t), and bridging-edge (be) H* sites.

S3. Images of the minimum energy pathway of filling Ir particles

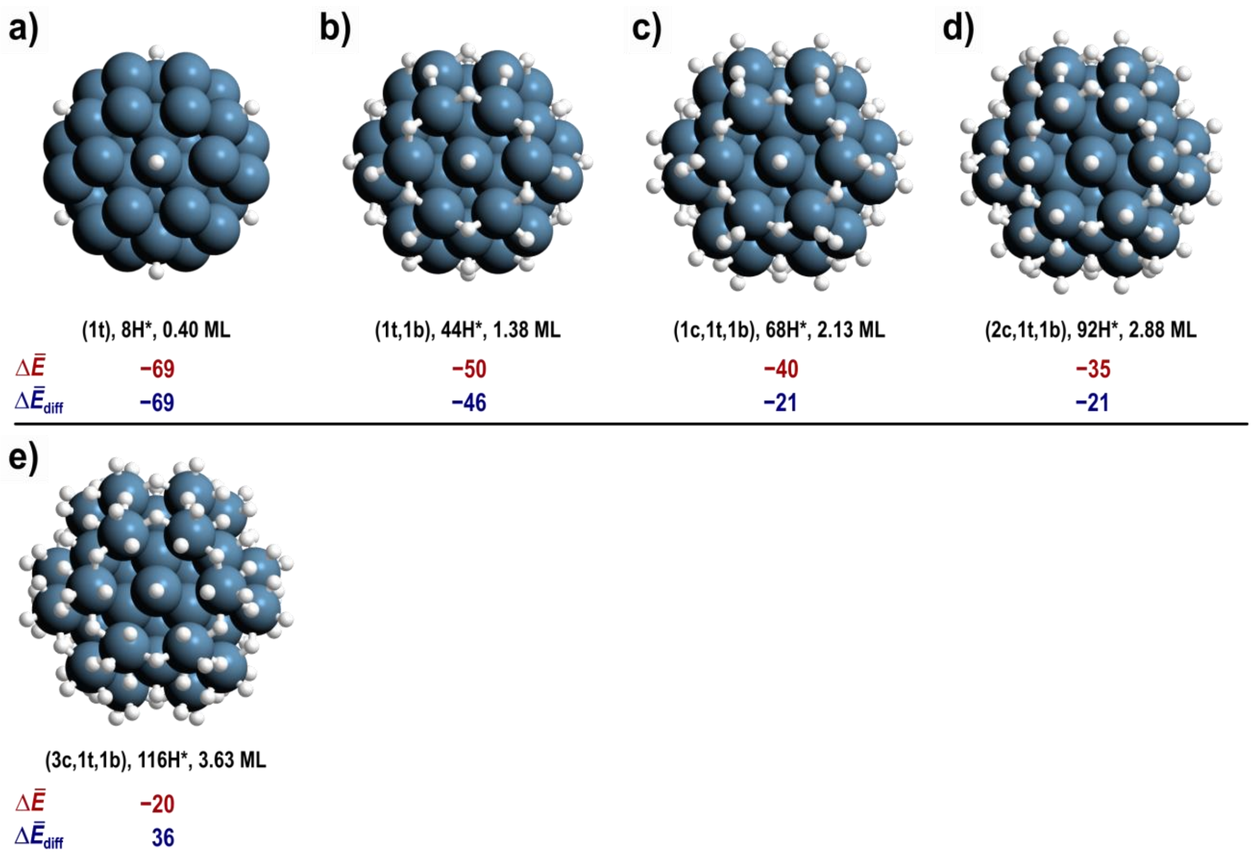

Figure S2. The minimum energy pathway of filling the Ir_{38} particle. Shown beneath each image are $\Delta\overline{E}$ (red) and $\Delta\overline{E}_{\text{diff}}$ (blue) in kJ mol^{-1}.

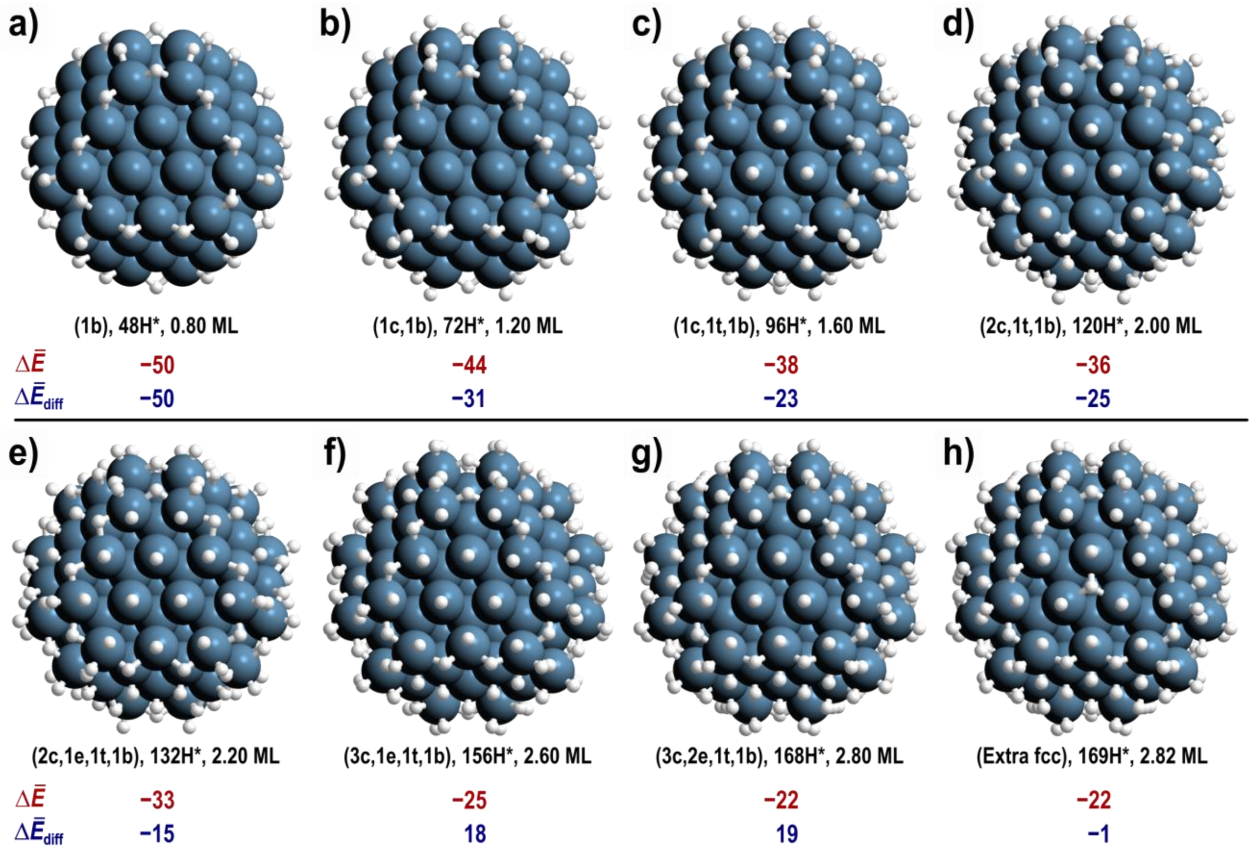

Figure S3. The minimum energy pathway of filling the Ir_{79} particle. Shown beneath each image are $\Delta\overline{E}$ (red) and $\Delta\overline{E}_{\mathrm{diff}}$ (blue) in kJ mol^{-1}.

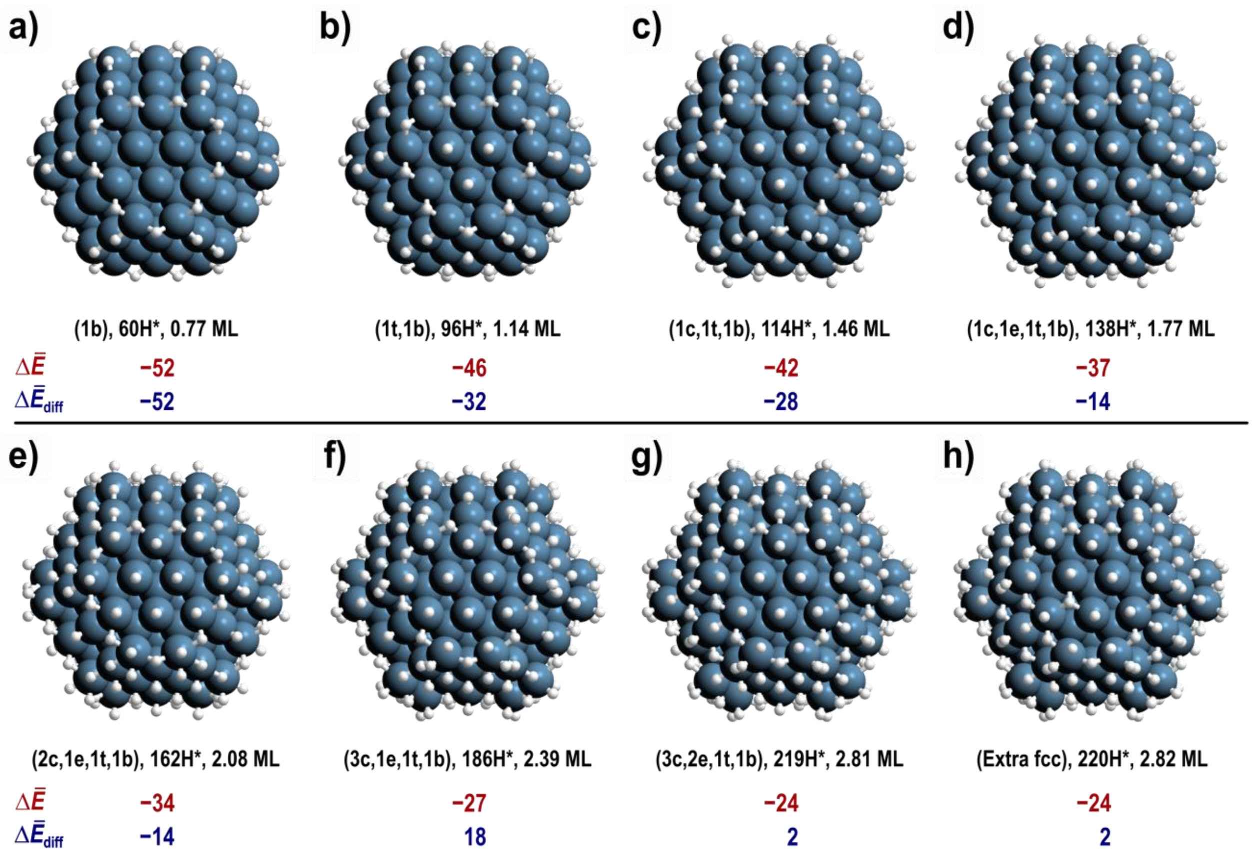

Figure S4. The minimum energy pathway of filling the Ir_{116} particle. Shown beneath each image are $\Delta\overline{E}$ (red) and $\Delta\overline{E}_{\mathrm{diff}}$ (blue) in kJ mol^{-1}.

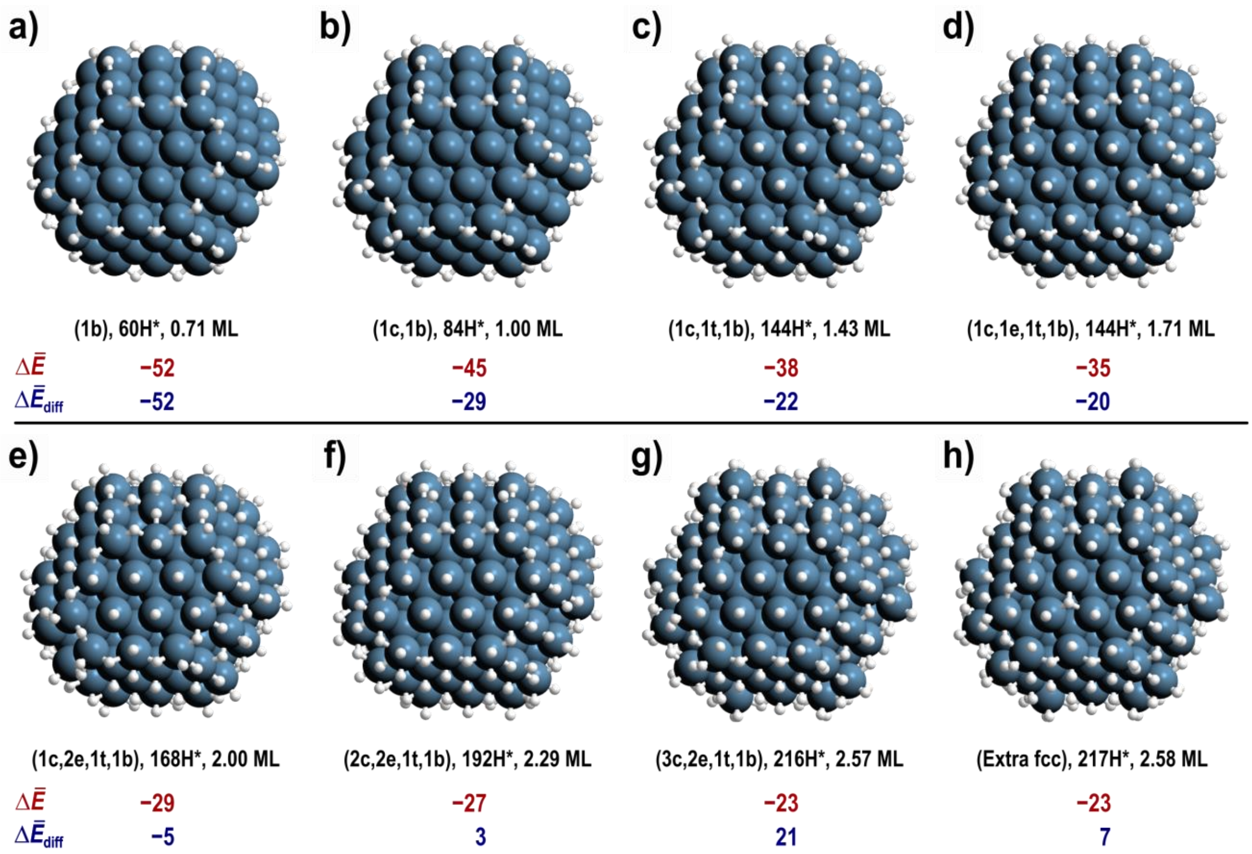

Figure S5. The minimum energy pathway of filling the Ir_{124} particle. Shown beneath each image are $\Delta\overline{E}$ (red) and $\Delta\overline{E}_{\mathrm{diff}}$ (blue) in kJ mol^{-1}.

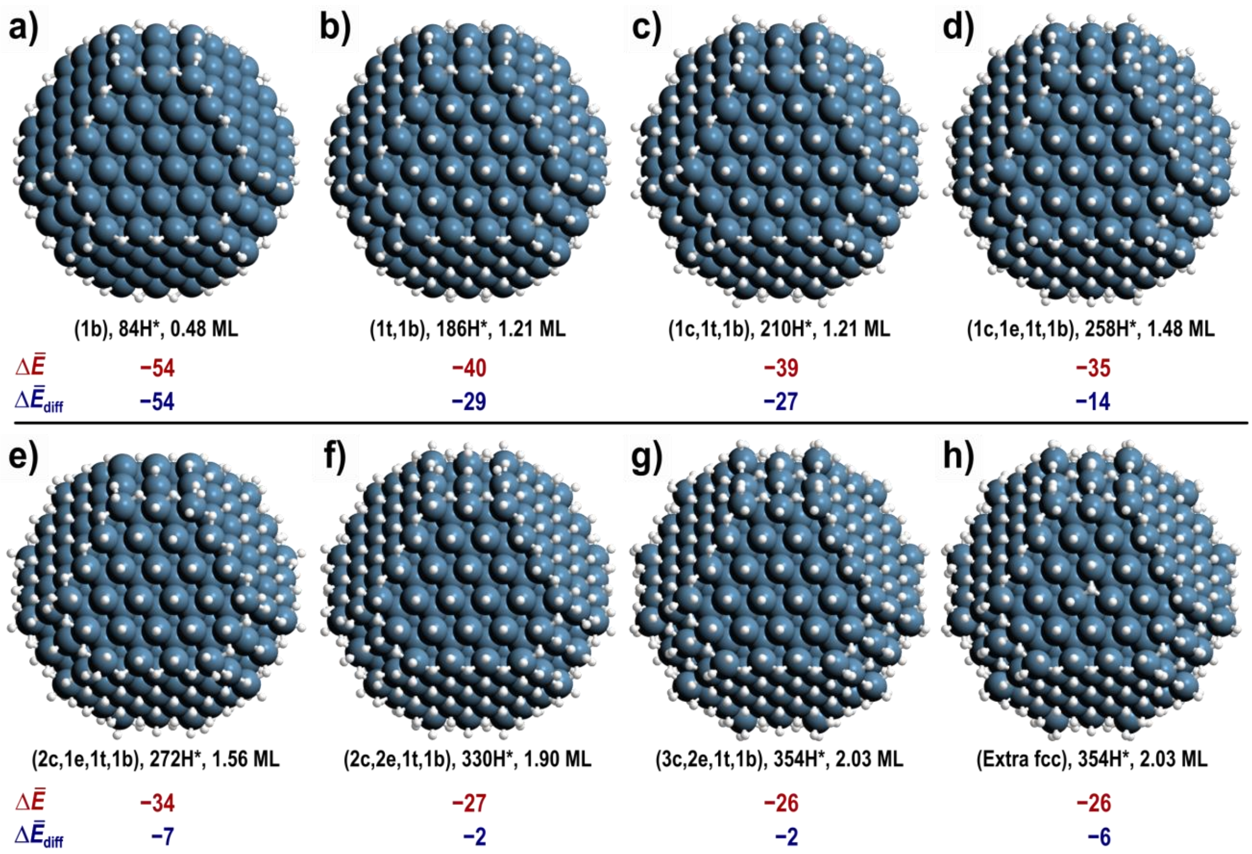

Figure S6. The minimum energy pathway of filling the Ir_{314} particle. Shown beneath each image are $\Delta\overline{E}$ (red) and $\Delta\overline{E}_{\mathrm{diff}}$ (blue) in kJ mol^{-1}.

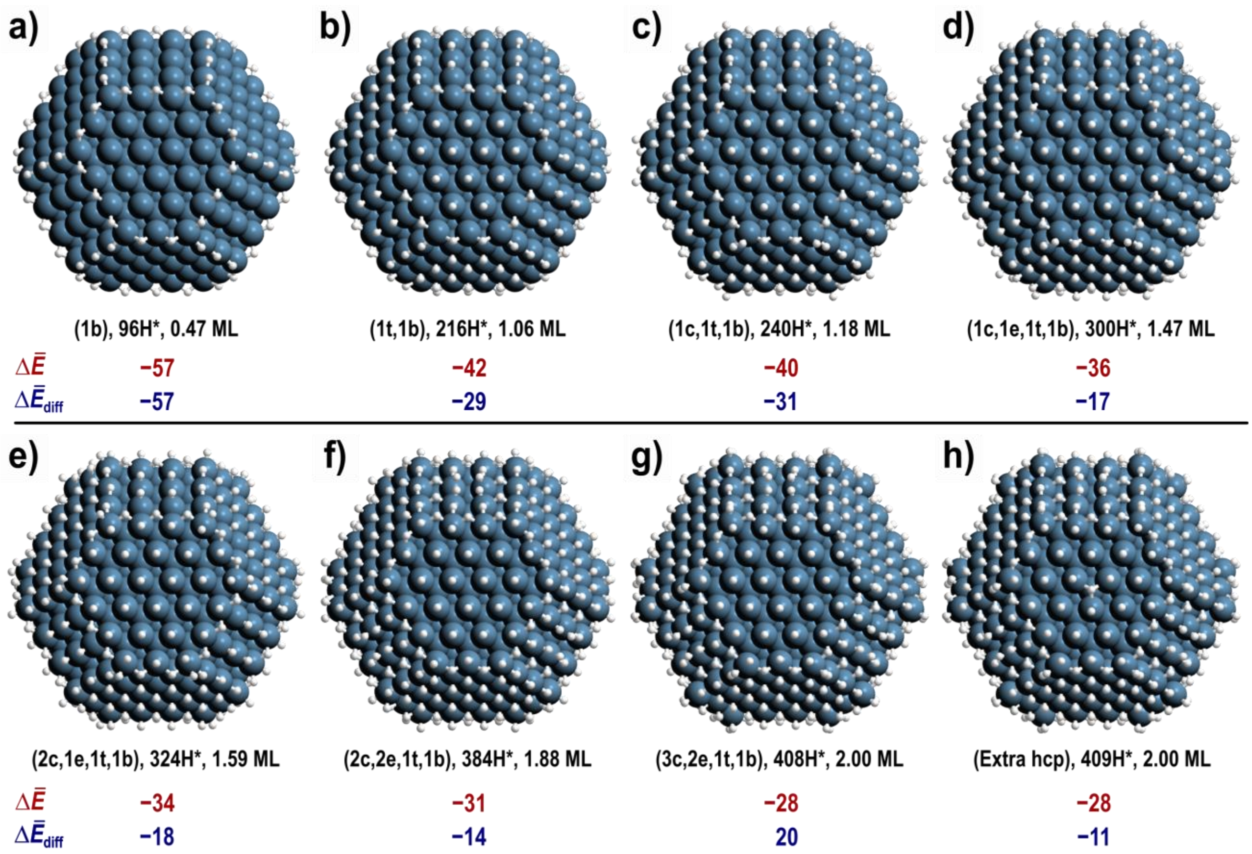

Figure S7. The minimum energy pathway of filling the Ir_{405} particle. Shown beneath each image are $\Delta\overline{E}$ (red) and $\Delta\overline{E}_{\mathrm{diff}}$ (blue) in kJ mol^{-1}.

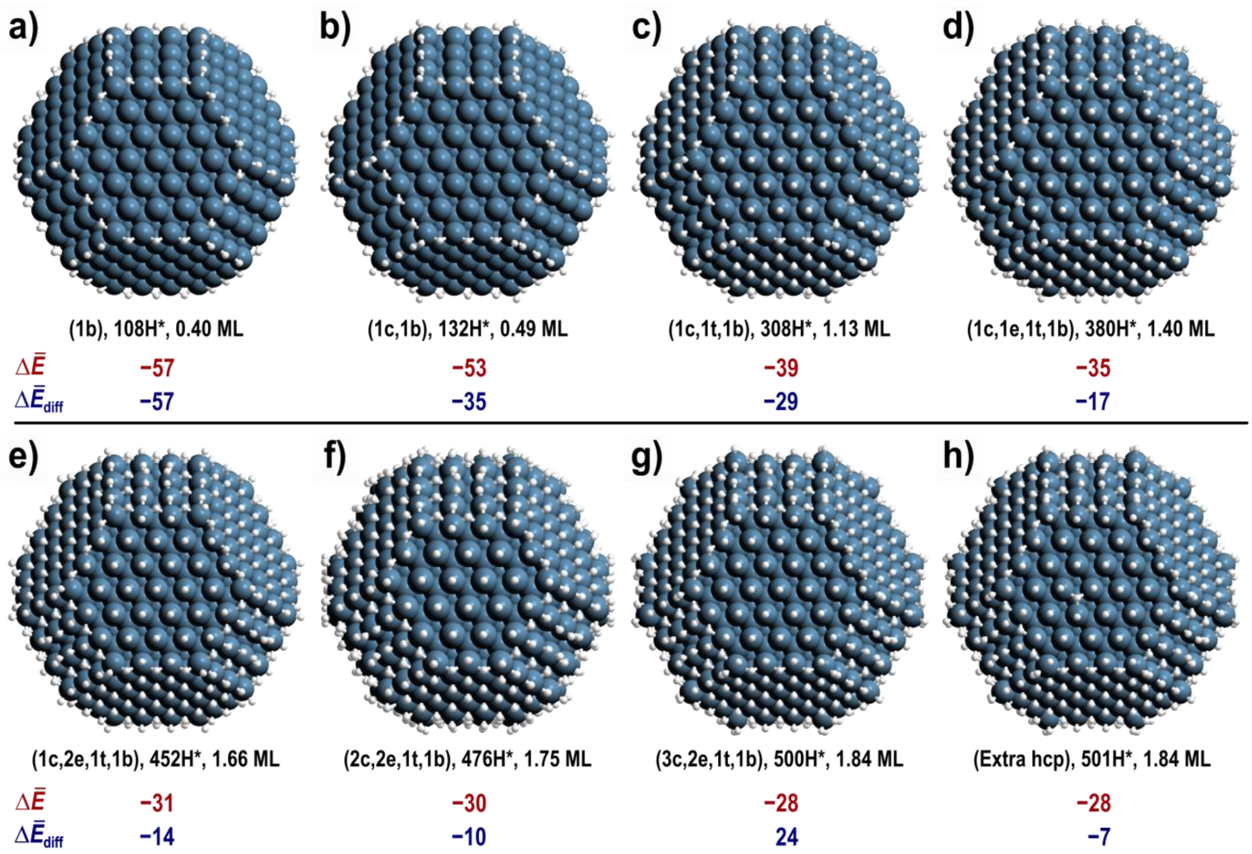

Figure S8. The minimum energy pathway of filling the Ir_{586} particle. Shown beneath each image are $\Delta\overline{E}$ (red) and $\Delta\overline{E}_{\text{diff}}$ (blue) in kJ mol^{-1}.

S4. Saturation coverages at ΔE_{diff}^{crit} for all Ir and Pt particles

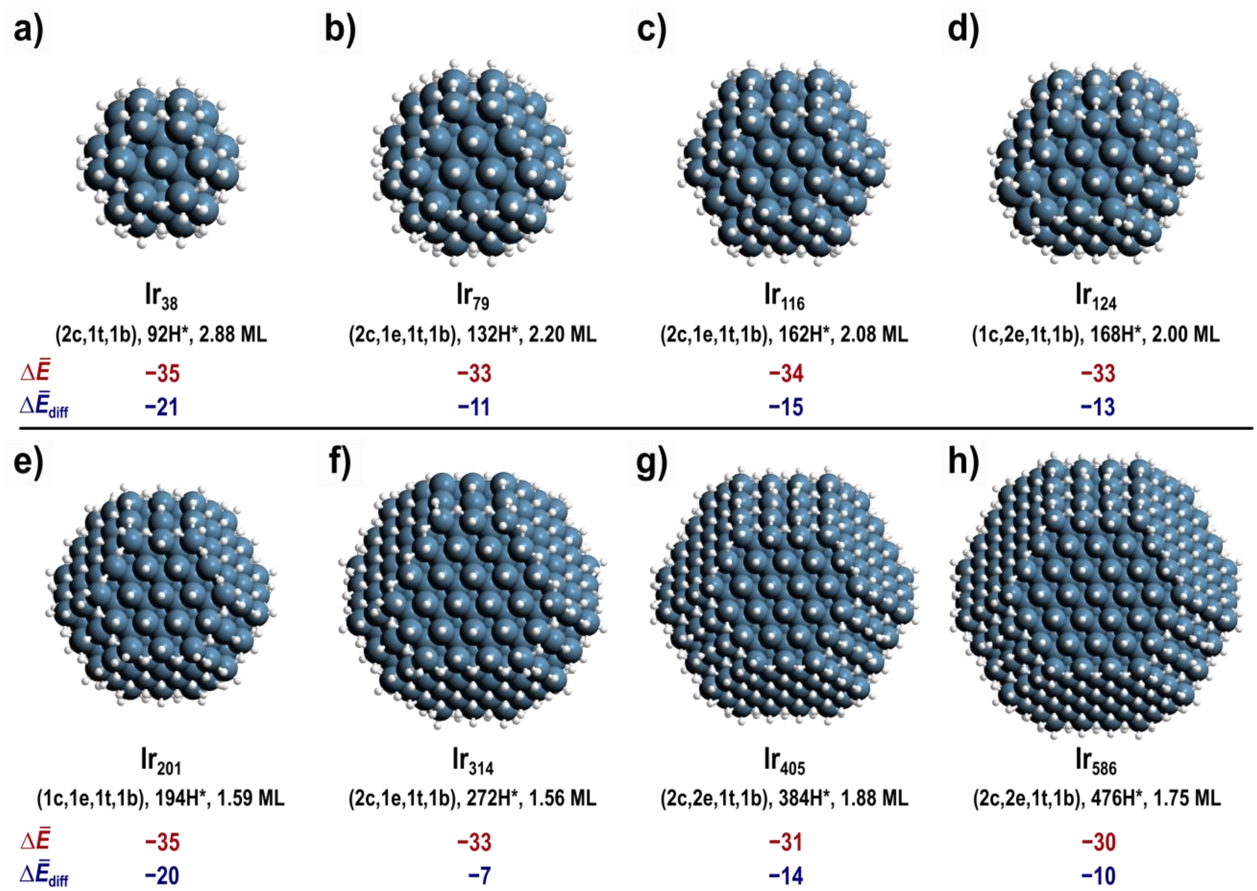

Figure S9. Saturation coverages at $\Delta E_{\mathrm{diff}}^{\mathrm{crit}}$ for all Ir particles. Shown beneath each image are $\Delta\overline{E}$ (red) and $\Delta\overline{E}_{\mathrm{diff}}$ (blue) in kJ mol^{-1}.

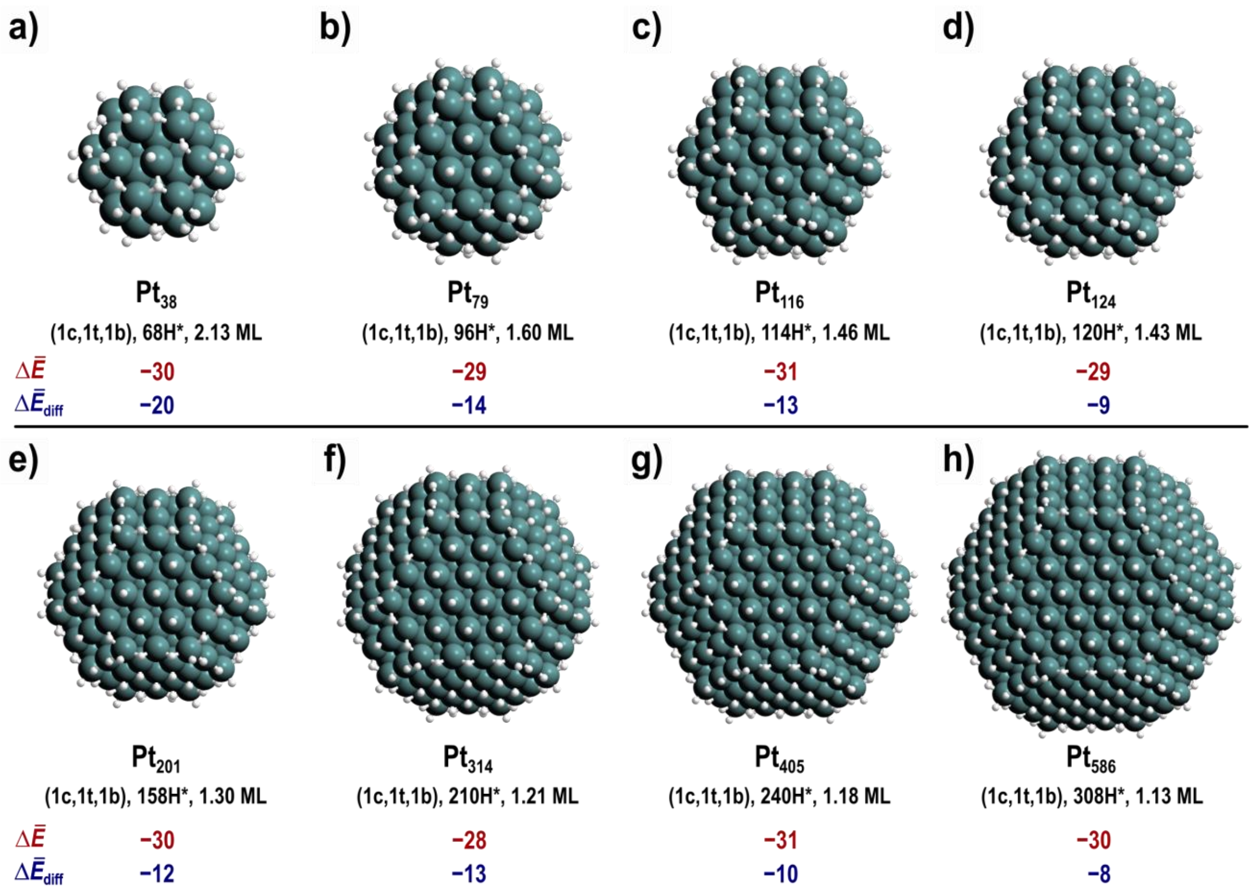

Figure S10. Saturation coverages at $\Delta E_{\text{diff}}^{\text{crit}}$ for all Pt particles. Shown beneath each image are $\Delta\overline{E}$ (red) and $\Delta\overline{E}_{\text{diff}}$ (blue) in kJ mol^{-1}.

S5. Effects of Corner/Edge H on Terrace H* Characteristics*

Here, we examine the effect of H* population on corners and edges on the binding energy of a single terrace H* atom without altering the coverage of all the other terrace sites. The binding energy of the central H* atom in Ir_{38} particle changes dramatically from −74 kJ mol^{-1} at 0.25 ML (1t) to −22 kJ mol^{-1} after the corner/corner bridging sites are filled (1t,1be, 1.38 ML) (Fig. S11a). The (111) terrace atoms on the Ir_{38} particle are directly adjacent to the corner atoms of the particle, as such, adsorbing H* to those undercoordinated atoms destabilizes the terrace H* atom via local through-surface interactions. The effect of increasing the coverage of corner atoms then becomes weaker and terrace H* binds with −16 kJ mol^{-1} in the fully covered state (3c,1t,1be, 3.63 ML). Large particles also do not exhibit a sharp change in terrace H* binding energy with increasing coverage of low-coordinated atoms (average of −20 kJ mol^{-1} at 0.5 ML and −16 kJ mol^{-1} at 2.0 ML), because the central terrace H* atoms being considered are not adjacent to the edges and corners of the nanoparticles and the through-space interactions among H* atoms are weak. Pt particles exhibit different trends and terrace H* binding energy weakens with increasing coverage even for large particles (Fig. S11b). The terrace H* binding energy changes from −68 kJ mol^{-1} at 0.25 ML (1t) to −19 kJ mol^{-1} at 2.88 ML (2c,1t,1be) on Pt_{38}. Larger particles also show a rapid change in the binding energy, in contrast to Ir particles. A terrace H* atom in Pt_{201}, for example, binds with −32 kJ mol^{-1} at 0.51 ML, which weakens to −1 kJ mol^{-1} at 2.08 ML. The effect of coverage on terrace H* binding energy starts to decrease with increasing particle size from Pt_{314} to Pt_{586}, where ΔE changes by less than 4 kJ mol^{-1} from 0.65 to 1.49 ML in Pt_{586}. These findings indicate that local through-surface interactions are stronger in Pt than in Ir.

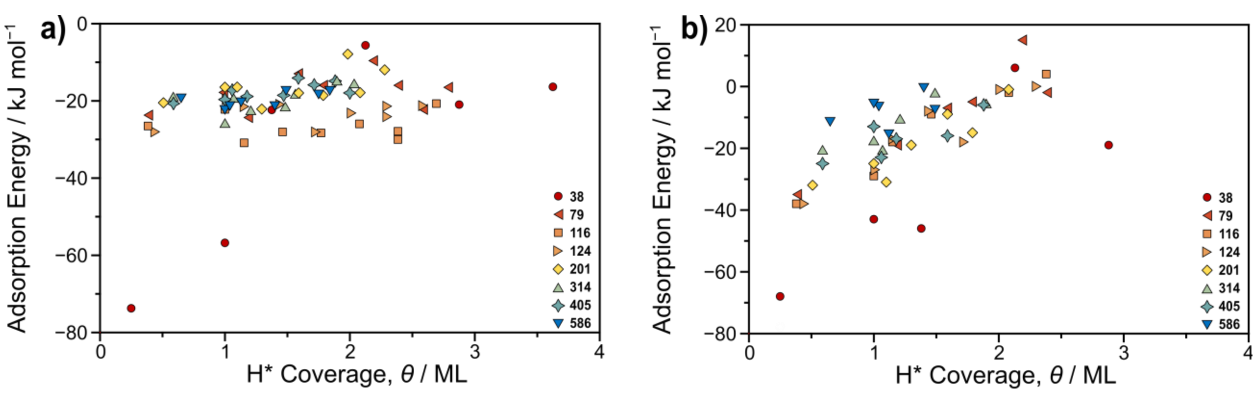

Figure S11. Effect of coverage on the binding energy of a single H* atom centered on (111) terrace in ***a)*** Ir and ***b)*** Pt particles.

S6. Effect of H coverage on M_s–M_s bond distance*

Average surface metal-metal bond (M_s–M_s) distance increases with increasing H* coverage in metal clusters, in contrast to single-crystal (111) surfaces (0.2716 and 0.2760 nm for Ir and Pt surfaces, respectively) (Fig. S12). M_s–M_s distance in Ir_{38}, for example, increases gradually from 0.2636 nm in the bare particle to 0.2653 nm at 1 ML, and then more rapidly to 0.2737 nm at 1.88 ML (Fig. S12a). H* coverage affects M_s–M_s distance less as the particle size increases; M_s–M_s distance in the large Ir_{586} particle changes by only 0.0044 nm from 0 to 1.84 ML. Notably, M_s–M_s distance in the bare Ir_{586} particle is much closer to that of the Ir (111) surface than the Ir_{38} M_s–M_s distance is to that of the (111) surface because (111) terraces represent the majority of the Ir_{586} surface. Average M_s–M_s distance in Pt particles also increases with increasing H* coverage but much more rapidly than in Ir particles at $\theta > 1$ ML (Fig. S12b); M_s–M_s distance in Pt_{38} changes by 0.0172 nm from 1 to 1.88 ML compared to 0.0101 nm in Ir_{38}.

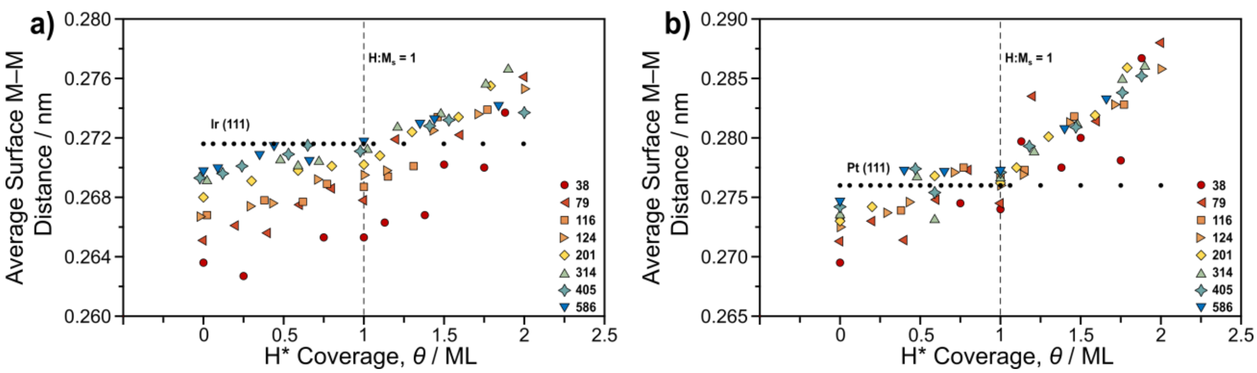

Figure S12. Average surface metal-metal bond distance as a function of H* coverage on ***a)*** Ir and ***b)*** Pt particles.